PAPER

Superpenumbral chromospheric flare

RAA 2018 Vol. **18** No. **10**, 130(10pp) doi: 10.1088/1674–4527/18/10/130

http://www.raa-journal.org *http://iopscience.iop.org/raa*

***R**esearch in*
***A**stronomy and*
***A**strophysics*

Superpenumbral chromospheric flare

Suo Liu[1], Hong-Qi Zhang[1], Debiprasad P. Choudhary[1,2], Abhishek K. Srivastava[3] and Bhola Nath Dwivedi[3]

[1] National Astronomical Observatories, Chinese Academy of Sciences, Beijing 100101, China; *debiprasad.choudhary@csun.edu*

[2] Department of Physics and Astronomy, California State University, Northridge, 18111 Nordhoff St, Northridge, CA, 91330, USA

[3] Department of Physics, Indian Institute of Technology (BHU), Varanasi-221005, India

Received 2018 April 24; accepted 2018 May 23

Abstract We observed a C-class flare at the outer boundary of the superpenumbra of a sunspot. The flare was triggered by an emerging magnetic bipolar region that was obliquely oriented with respect to the superpenumbral fibrils. The flare started due to the low height magnetic reconnection of emerging magnetic flux with a superpenumbral field resulting in hot multi-temperature plasma flows in the inverse Evershed flow channel and its overlying atmosphere. Inverse Evershed flows in the chromosphere start from the superpenumbra towards the sunspot that end at the outer boundary of the penumbra. The hot plasma flow towards the sunspot in the inverse Evershed channels show about 10 km s^{-1} higher velocity in Hα wavelengths compared to the plasma emissions at various temperatures as seen in different AIA filters. Even though these velocities are about seven times higher than the typical inverse Evershed flow speeds, the flow is diminished at the outer boundary of the sunspot's penumbra. This suggests that the superpenumbral field lines that carry inverse Evershed flows are discontinued at the boundary where the penumbral field lines dive into the sun and these two sets of field lines are completely distinct. The discontinuity in the typical magnetic field and plasma properties at the adjoining of these two sets of field lines further leads to discontinuity in the characteristic magnetoacoustic and Alfvén speeds, thereby stopping the plasma flows further on. The multi-temperature plasma in the inverse Evershed channels exhibits possible longitudinal oscillations initially during the onset of the flare, and later flows towards the sunspot. In the multi-temperature view, the different layers above the flare region have a mixture of supersonic as well as subsonic flows.

Key words: magnetic field — solar flare — trigger — magnetic emergence

1 INTRODUCTION

Solar flares occur near intense magnetic field regions that contain sunspots. We obtained high resolution chromospheric observations of a solar flare in the superpenumbra of a sunspot that help understand both the trigger mechanism of small flares and the structure of the sunspot. This paper addresses both the trigger mechanism of small flares and structure of the associated sunspot.

Solar flares are most likely caused by a sudden release of magnetic energy due to plasma instabilities or magnetic reconnection (Hahn et al. 2005). For large solar flares it is known that energy storage can be achieved by twisting the magnetic field due to foot point motion and/or twisted flux emergence, and the trigger for large flares is due to flux emergence (Hagyard & Rabin 1986; Choudhary et al. 1998; Gary & Moore 2004; Wang et al. 2008). Falconer et al. (2009) showed that the magnetic field configuration of active regions explodes after achieving their maximum attainable free energy in order to reach the equilibrium state. Several studies have shown

evidence of the chromospheric origin of explosive event activity (Doyle et al. 2005; Fletcher 2010). This is especially true for smaller flares. While large flares are well studied, the locations of the trigger mechanisms for small flares are not clear. The event presented here gives an opportunity to study the trigger mechanism and its location in the chromosphere.

We also use this event to study the sunspot structure by observing the flow of hot flare plasma along fine structures around sunspots. Sunspots consist of magnetic flux bundles that protrude through the photosphere and expand into the chromosphere and corona. Magnetic field lines in the umbra are mostly vertical and inclined to various degrees in the penumbra and superpenumbra, floating above the photosphere in an uncombed fashion (Martínez Pillet 2000). The penumbral-fibrils carry Evershed flows that mostly terminate in a ring of downflow channels at the outer edge of the boundary with the quiet sun (Schlichenmaier & Schmidt 1999). About a 10th of penumbral field lines extend beyond the boundary carrying the Evershed flow material and rise up into the superpenumbral magnetic canopy that surrounds a sunspot some 300 km above the photosphere (Westendorp Plaza et al. 1997; Solanki et al. 1992; Rueedi et al. 1992). Extensive studies of photospheric Evershed flows along penumbral fibrils show that the inclined magnetic field from the spot mostly dives down into the photosphere at the penumbral boundary, but its connection to the superpenumbra is less clear primarily due to the paucity of chromospheric inverse Evershed flow. These flows are carried by fibrils that exist in a superpenumbra. The photospheric region corresponding to the superpenumbra is observed with moat flows and moving magnetic features along the direction of penumbral filaments. The superpenumbral fibrils are observed in the chromosphere, carrying inverse Evershed flow material towards the spot at speeds of about 8–10 $\mathrm{km\,s^{-1}}$ (Georgakilas et al. 2003). Most superpenumbral fibrils terminate at the boundary of the penumbra-quiet sun and about one third of them begin inside the umbra (Louis et al. 2014; Balasubramaniam et al. 2004).

In the three dimensional solar atmosphere, a superpenumbral filament may form the upper boundary layers of the associated canopy, therefore, it may lie in the upper chromosphere and transition region. There have only been a few reports in the past which describe inverse Evershed flows at the transition region temperature (Teriaca et al. 2008), while most of the flows are observed in the lower solar chromosphere (Vissers & Rouppe van der Voort 2012). Recently, evidence for an accelerated flow ($\approx$40 $\mathrm{m\,s^{-2}}$) along a fibril anchored at its endpoints in the outer boundary of the sunspot and weaker plage supports the magnetic siphon flows and its role in the formation of the inverse Evershed effect in the solar chromosphere (Schad et al. 2013). Beck et al. (2014) found evidence that inverse Evershed flows occur into a sunspot in the lower chromosphere due to the siphon flows along short quiescent loops.

These observations suggest that most of the inclined field channels associated with a sunspot dive into the photosphere carrying downflow plasma at the boundary of penumbra and superpenumbra. The structure of magnetic field arrangement in this region, therefore, is an important aspect of the overall sunspot structure as penumbral and superpenumbral structure could contain separate sets of field bundles that enable mass transfer due to different mechanisms. The magnetic field structure has been studied in detail in the outer periphery of the spots, which may provide more detailed information about the flows there. There are various views on it, *viz.*, Schad et al. (2015) have shown that the superpenumbral magnetic field does not appear to be finely structured, unlike the observed intensity structures indicating that the fibrils are not concentrations of magnetic fluxes; instead they are distinguished by localized thermalization. On the other hand, the actual sunspot penumbra is considered to be inter-combed with finely structured magnetic fields due to the downward pumping of the fluxes (Thomas 2002). The normal Evershed effect is associated with the magnetoconvection and the sunspot penumbral regions (Ichimoto et al. 2007). It was found that the weaker dark regions in-between penumbral filaments of the spot are the likely regions for upward Evershed flows in the lower solar chromosphere (Bellot Rubio et al. 2007). Therefore, in the spot's penumbra, this effect may be nonlinear magnetoconvection that has the properties of traveling waves in the presence of a strong, highly inclined magnetic field (Kitiashvili et al. 2009).

Considering that the superpenumbra is not a mere finely structured magnetic tube, but instead is a thermalized atmosphere supplemented by a bulk magnetic field which consists of outward (e.g., localized jets) and inverse plasma flows (e.g., inverse Evershed effects), study of such plasma dynamics and their drivers has become significant in such regions from hydrodynamic (or magnetohydrodynamic) point-of-views, which circulate mass

and energy. As stated above, there are only a few studies, especially targeting the solar chromosphere, which have taken into account the physical processes involved in triggering inverse Evershed flows in the superpenumbral regions.

To the best of our knowledge, this is the first attempt to unveil the multi-temperature view of the inverse Evershed flows in superpenumbral regions around a sunspot to understand the underlying physical processes in their formation. In this paper, we probe this region by studying the flow of heated plasma resulting from a C-class flare at the outer superpenumbral boundary. Section 2 describes the observational data and related analyses. We outline the observational results and their interpretation in Section 3. The last section provides the discussion and conclusions of this paper.

2 OBSERVATIONS AND ANALYSIS

The event studied in this paper is a C-class flare which occurred at 3:38 UT in NOAA 11598 located at S12E15 on 2012 October 25. In this study, we utilize time-lapse high resolution images through an Hα filter, and images in ultraviolet wavelengths formed at transition region heights above the sunspot. The Hα observations are obtained with the New Vacuum Solar Telescope (NVST) located at Fuxian Solar Observatory (FSO) in southwest China. The telescope with its 985 mm aperture was designed as a modified Gregorian system which has an effective focal length of 45 m (Liu et al. 2014). The main goal of NVST is to reveal fine structures in both the photosphere and chromosphere through spectral and imaging observations with high spectral and spatial resolution in the wavelength range from 0.3 to 2.5 micron. The NVST has mainly provided Hα (656.3 nm with passband 0.025 nm) and TiO (705.8 nm with passband 0.01 nm) data for observing the chromosphere and photosphere, respectively. Generally, the observational data are processed from Level 0 to Level 1 through dark current subtraction and flat field correction, then reconstructed to Level 1+ by the method of speckle masking (Weigelt 1977). After image reconstruction, the Hα image has resolution of 0.162 arcsec pixel^{-1} and cadence of 12 s for scientific analysis. The processed sequence of Hα images is used to make a movie that can be seen in event.mpg. The high resolution image of the first frame shows the umbra, penumbra and superpenumbra structure around the sunspot. The movie indicates that following a flare at the boundary of the superpenumbra, the Hα emission moves towards the spot along the superpenumbral fibrils and stops at the penumbral edge.

In order to study the dynamical process of the event, we use data obtained with the Atmospheric Imaging Assembly (AIA) and Helioseismic and Magnetic Imager (HMI) onboard the *Solar Dynamics Observatory* (*SDO*) (Lemen et al. 2012; Schou et al. 2012; Pesnell et al. 2012). The images from AIA 304 Å, 171 Å and 211 Å channels, with a resolution of 0.6″ pixel^{-1} and a cadence of 12 s, are used for this study. The line-of-sight (LOS) magnetograms with a resolution of 0.6″ pixel^{-1} and a cadence of 45 s with HMI are used to study the magnetic field configuration of the flaring site and the surrounding area. The data processing is based on the standard Solar Softwares (SSW) related to these instruments (such as hmi_prep.pro, aia_prep.pro and drot.pro). For observation alignment, image cross correlation is applied to match the features between the AIA 304 Å and Hα, while AIA and HMI can be aligned through exact position and time observed information. Additionally, the high resolution G band 4304, Ca II and Na I observation obtained from Solar Optical Telescope (SOT)/*Hinode* is also used in this work (Kosugi et al. 2007; Tsuneta et al. 2008). G band 4304 and Ca II H line data with high resolution of 0.21 arcsec pixel^{-1} can reveal fine structures of the photosphere and chromosphere, respectively, while Na I 5896 Å line observation with resolution of 0.32 arcsec pixel^{-1} from SOT/*Hinode* can trace the LOS magnetic field that slightly approaches the photosphere, which can be used as a supplement for the HMI magnetic field to display structures and evolution of the magnetic field of interest. The *Hinode* data processing is also based on SSW (*e.g.*, fg_prep.pro), where dark subtraction, flat fielding, the correction of bad pixels and cosmic-ray removal were done for filtergram images obtained by SOT.

3 OBSERVATIONAL RESULTS

Figure 1 shows the Hα image and corresponding photospheric magnetogram of the sunspot and surrounding region. The encircled region in Figure 1(a) is the site of initial brightness of the flare, which is characterized by a narrow field structure with opposite polarity compared to its surrounding.

Figure 1 displays a quadrupolar magnetic configuration at the location of the initial brightness of the flare that is indicated by a circle on the *SDO*/HMI (middle panel (b)) and Na I (right panel (c)) snapshots. In the Hα

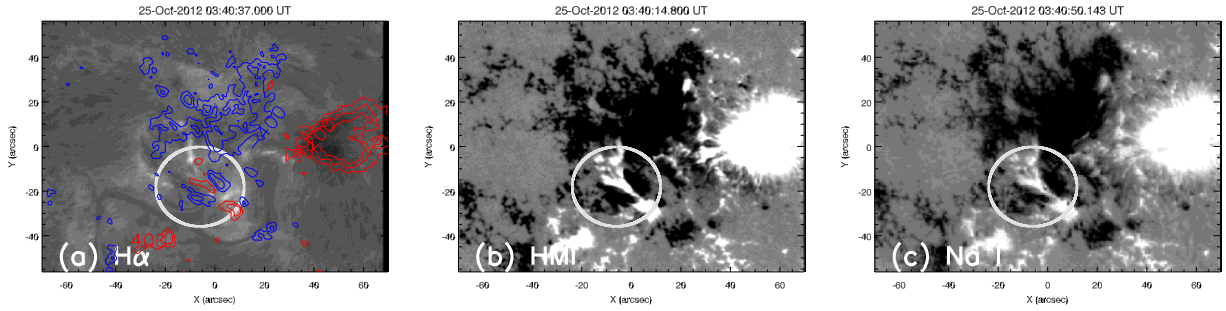

Fig. 1 *Left panel* (a) Hα image obtained by the NVST with LOS magnetic field contours on 2012 October 25 at 03:40 UT. *Middle panel* (b) HMI LOS magnetic field where *red* is positive while *blue* is the negative. *Right panel* (c) Na I line observation indicating LOS magnetic field similar to that of HMI. The *white circles* drawn in (b) and (c) is the region-of-interest where the inverse Evershed flows are identified.

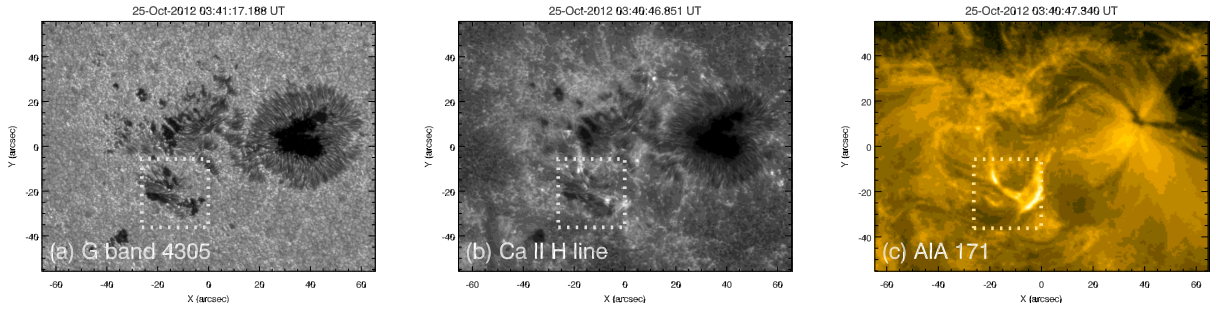

Fig. 2 G-band image (*left panel*) and Ca II H image (*middle panel*) obtained with the SOT onboard the *Hinode* mission, and AIA 171 Å image (*right panel*) observed by *SDO*. Brightness is observed at the polarity inversion channel of the emerging flux region. The Ca II image shows a dark pore structure at the same location.

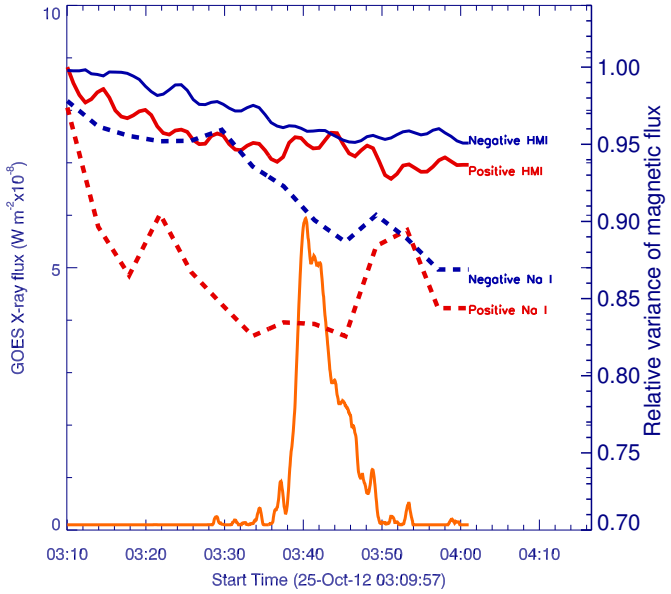

Fig. 3 The *solid lines* show evolution of photospheric magnetic flux observed with the 6301.2 Fe I line and the *dotted lines* indicate lower chromospheric magnetic flux observed with the Na line, which corresponds to the subregion labeled by the *white circles* in Fig. 1. The flux of X-ray obtained from *GOES* is appended for a comparison of various phases of the C-class flare.

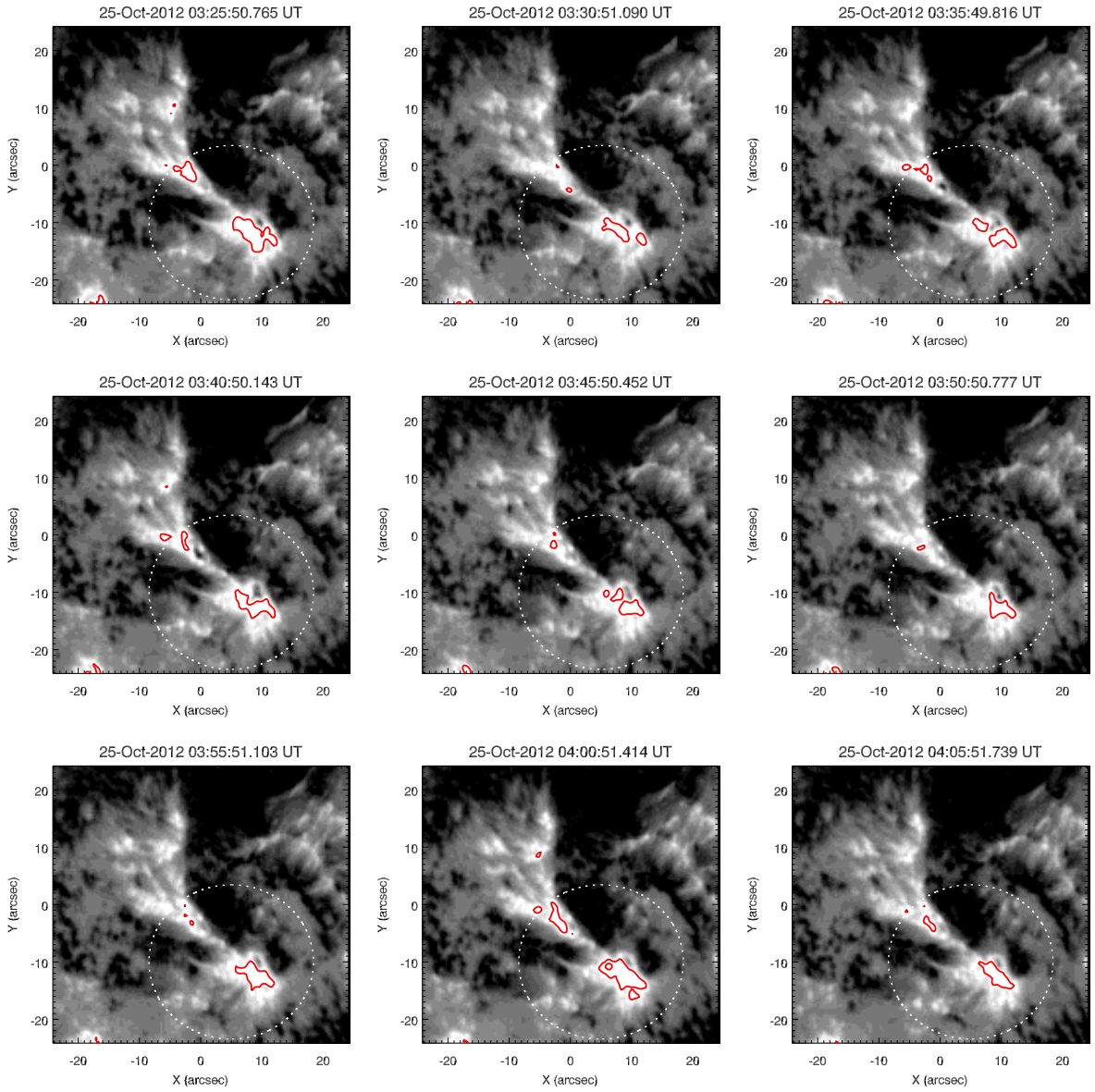

Fig. 4 A time series image of the Na line with corresponding contours obtained for SOT/*Hinode* observations. The *white circle* drawn in each panel indicates the region-of-interest where inverse Evershed flows are identified, the same as in Fig. 1.

image, the bright fibrils of the superpenumbra are visible, which seem to terminate at the outer boundary of the positive polarity sunspot at its northern side.

Figure 2 features images of the same area in G-band and Ca II obtained by SOT onboard the *Hinode* mission and the AIA 171 Å image observed by *SDO*. The G-band and 171 Å brightening in the location of flare and absence of Ca II structure suggest the presence of an intense vertical magnetic field at this location.

Figure 3 depicts the evolution of magnetic field near the flare location as a function of time. Here the relative values of magnetic flux are plotted, which are normalized to the initial time (03:10) in this plot. At the mean time *GOES* X-ray flux is added to the labeled flare process, the positive and negative magnetic fluxes are calculated. The flux cancelation prior to the flare onset and emergence around the flare time is clearly evident from the relative variance of positive and negative flux.

Figure 3 illustrates the evolution of the LOS magnetic field, where the flux is seen to be decreasing unevenly, indicating emergence and cancelation on the flare site. The circular polarization signals in the Na line,

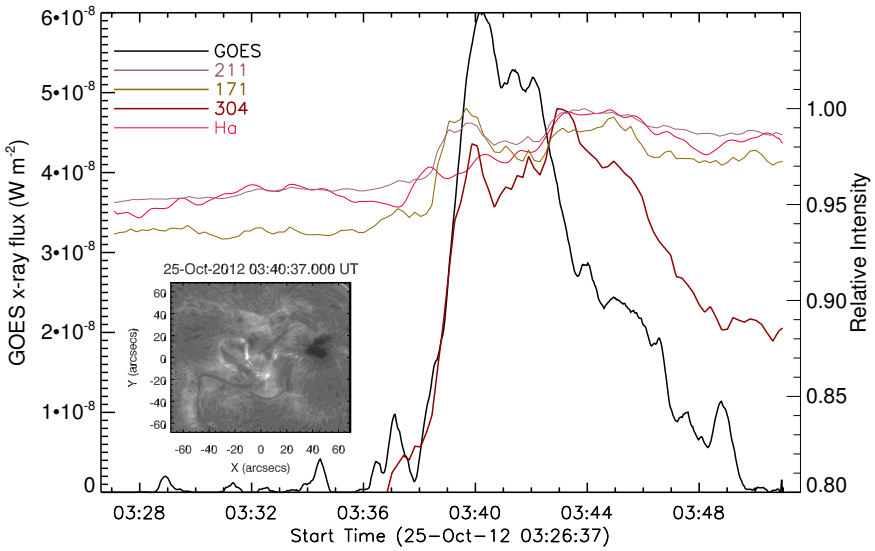

Fig. 5 This shows the evolution of Hα, *GOES*, and AIA: 304 Å, 171 Å and 211 Å flux for the corresponding labeled field of view.

which represent the magnetic flux in the lower chromosphere, also exhibit a similar trend, except that there was an apparent imbalance of signal representing negative and positive fields. The flare should be regarded as it was triggered by small scale magnetic structure highlighted by the white circles plotted in Figure 1, and the evident variances of this local magnetic field reflect its trigger potentiality for this small flare and subsequent high speed plasma flow. We might conclude the emerging flux is tilted such that even at chromospheric height negative flux is seen to be enhanced. The flux cancelation continuously heated the localized plasma that moved along the superpenumbral fibrils towards the sunspot. As the new flux emerges below the superpenumbral canopy, it might reconnect with the pre-existing magnetic field lines above.

We describe such a situation, illustrated in Figure 8, in a detailed manner in the forthcoming paragraphs. Additionally, to depict the evolutions of magnetic fluxes more intuitively, the polarization signals in Na line with contours are shown in Figure 4 based on the time series observations. From the distributions of contours in Figure 4, it can found that before the flare there were evident decreases in magnetic fluxes.

Figure 5 shows the light curve of the flaring region in *GOES* X-ray superimposed with Hα and other wavelengths obtained by integrating the inserted field of view. The time difference between the peak of the light curve is less than 2 seconds, which is a typical scenario for compact flares (e.g., Benz, 2008; Shibata and Magara, 2011; Benz 2008; Shibata & Magara 2011). In order to obtain the speed of the flare heated plasma, time-slice images are prepared by stacking the images along two slits aligned with the superpenumbral fibrils, as displayed in Figure 6. The speeds of the brightness propagation in Hα and AIA images obtained from the time-slice images are summarized in Table 1. The speeds in images in the transition region are about 10 km s^{-1} lower than the speed in Hα images. As a reference in Figure 7, we depict the pre-flare phase where such flows are absent.

Table 1 Velocity of the Propagation of Brightness in Hα and AIA Images

Slit Position	Hα	AIA 304 nm	AIA 171 nm	AIA 211 nm
		(km s^{-1})		
S1	69.52	62.50	61.44	61.83
S2	99.50	90.62	93.98	84.58

Figure 8 illustrates the heating of chromospheric material and the propagation geometry in the form of a diagram. The near simultaneous occurrence of light curve peaks in different wavelengths exhibited in Figure 3 suggests a low altitude reconnection event with the X-line shown in the figure, which is initially located in the chromosphere and then rapidly moves upward (Forbes 2003). Similar events resulting from low altitude with different magnitude have been observed with the *Solar Maximum Mission* (*SMM*) (Antonucci et al. 1990).

From the photospheric magnetic field configuration and appearance of initial brightening, it is clear that the plasma heating site was located near the outer edge of the superpenumbra. As the X-point moved rapidly up-

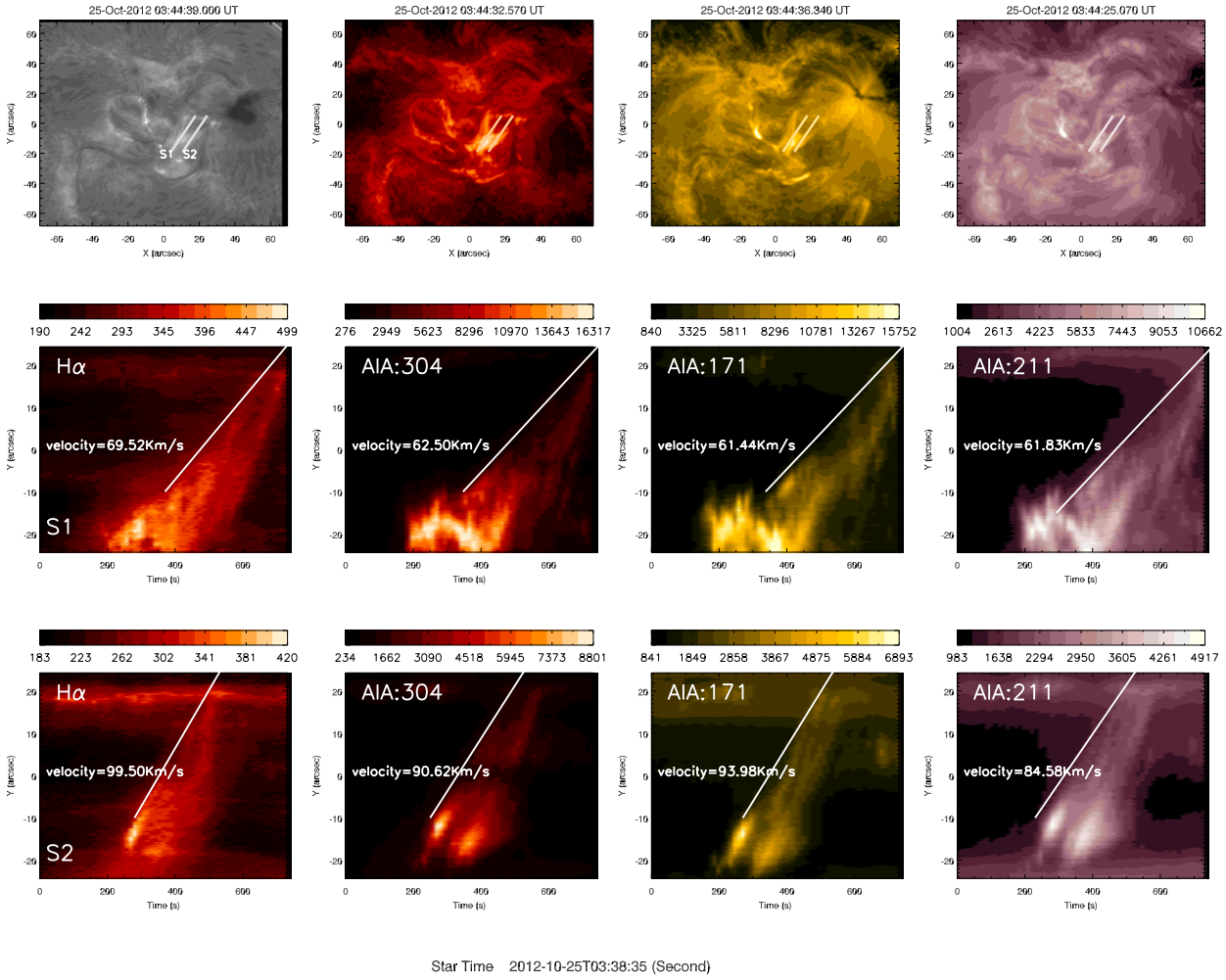

Fig. 6 Hα and AIA: 304 Å, 171 Å and 211 Å time-distance plots for two slits selected from an individual image. The *slanted line* in each panel is used to illustrate the labeled velocity.

ward into the chromosphere and transition region forming a current sheet, the hot plasma got loaded on to the magnetic field lines delineating superpenumbral fibrils and moved towards the penumbra in the same pattern as an inverse Evershed flow. If we consider the proper motion speeds of the bright front as representative of the mass motion of heated material, the speeds in Hα are found to be around 60 to 90 km s^{-1} and the transition region speeds are about 10 km s^{-1} lower, as can be seen in Table 1. These speeds are about 10 times higher than the normal inverse Evershed flow speeds.

When we analyze the inverse Evershed flows in the lower temperature band, the Hα movie of the flare shows that the brightness moves from the heating site towards the sunspot and stops at the boundary marking the penumbra and superpenumbra. No brightness is observed in the penumbral region represented by grey lines in the diagram. It is remarkable to notice that even though the plasma moved at a speed that is about 10 times higher than the speed of inverse Evershed material, it did not penetrate the umbral region, as apparent in the movies in Hα and AIA wavelengths. This would imply that the superpenumbral fibrils carrying hot plasma terminate at the boundary where the umbral fibrils also dive into the sun and these two sets of magnetic field lines do not inter mingle. The barrier at this boundary is so strong that the high speed plasma cannot be overcome.

4 DISCUSSION AND CONCLUSIONS

To the best of our knowledge, this is the first attempt to study the multi-temperature view of inverse Evershed flows in and above the superpenumbral regions around a sunspot. As observed, during the onset of the flare, the speed of heated plasma in Hα is found to be around 60

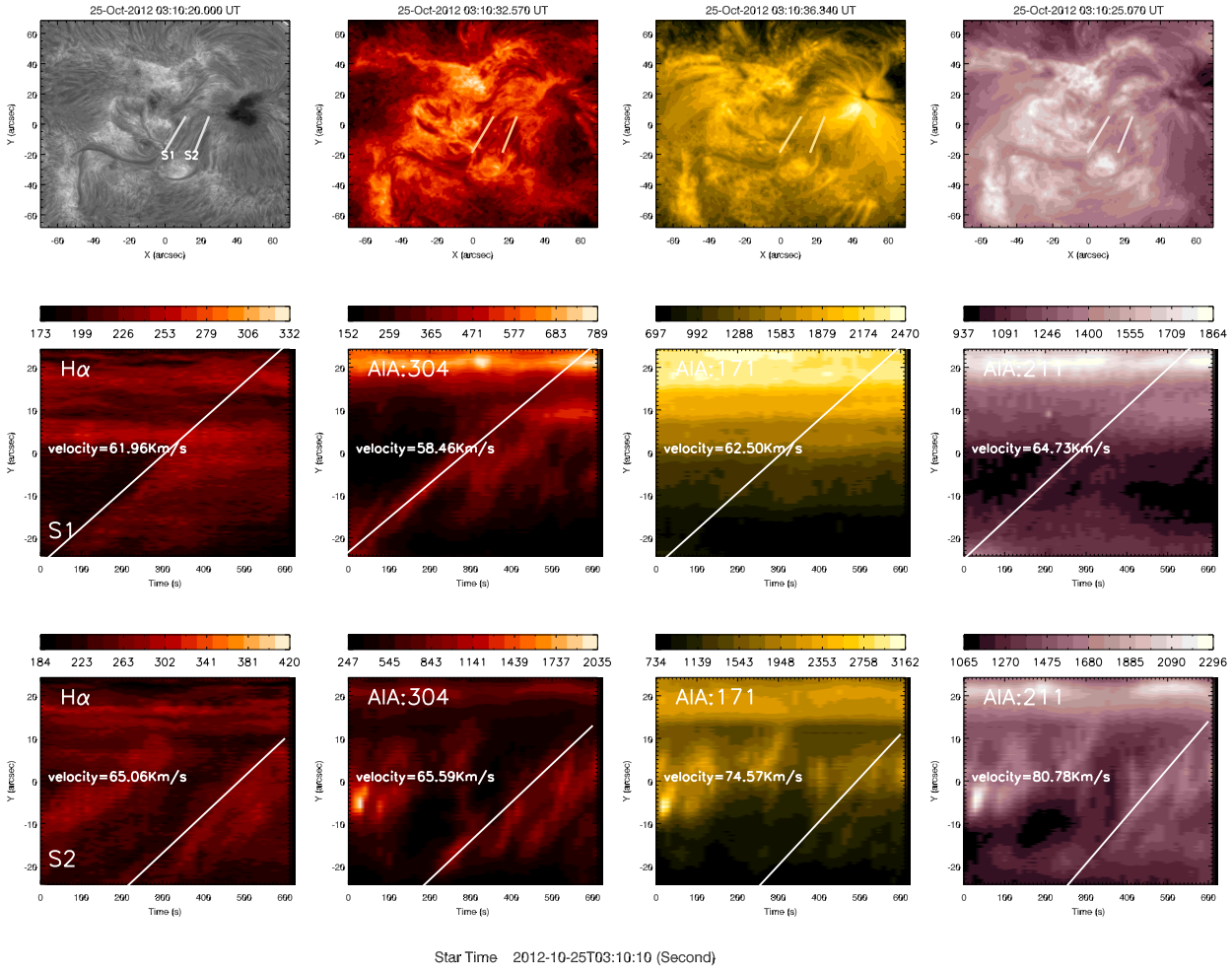

Fig. 7 Hα and AIA: 304 Å, 171 Å and 211 Å time-distance plots for two slits selected from an individual image obtained in a quiet phase of the pre-flare stage. The *slanted line* in each panel is used to illustrate the labeled velocity.

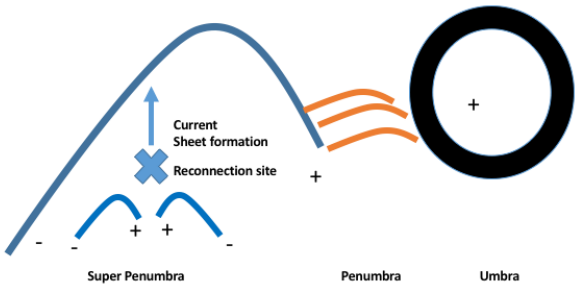

Fig. 8 Model of the event. The *dark thick circle* represents the positive polarity sunspot umbra. The *maroon colored arches* signify the penumbral fibrils. *Blue colored superpenumbral arch* originates at the boundary of penumbral fibrils and extends to the mote region. The two *blue arches* below the superpenumbra stand for the emerged flux that creates an "X" point, which is a site of chromospheric reconnection. The hot plasma produced as a result of reconnection moves upwards as shown by the *arrow mark*.

to 90 km s^{-1} and the speeds in the transition region and inner coronal layers are a few tens of km s^{-1} (Table 1). These speeds are about five times higher than the normal inverse Evershed flow speeds. In spite of large speeds, even these flows are stopped at the boundary of the spot's penumbra like normal inverse Evershed flows.

Due to the different scale heights and density stratification in the solar atmosphere, these oppositely directed flows have a less direct relationship with the photospheric Evershed effect (Teriaca et al. 2008). In fact, these dynamics are the set of down flowing plasma from the top of the canopies in the superpenumbral region, which may sometimes be mixed with the chromospheric inverse Evershed flows. At the Hα formation temperature, the observed speed falls at a supersonic scale between 60–90 km s^{-1}, which is larger than the typically observed speed of the inverse Evershed flows in the chromosphere (Schad et al. 2013). When we study the flows detected at different temperatures, e.g., transition region to inner corona in the same region, the flow speeds switch towards subsonic (Table 1). Therefore, the multi-temperature view of this flow is a mixture of supersonic and subsonic plasma motions drifting towards the penumbra of the northward sunspot (Figs. 1 and 6). The higher speed of the inverse Evershed flows may be due to the modulation of flare energy release as well as changing magnetic field and plasma conditions at the site where they originated.

Although the flows at multi-temperature plasmas were ongoing, we also notice that the overlying loop-system, visible at transition region and inner coronal temperatures (Fig. 6) at the flare site on top of it (Fig. 8), exhibits possible longitudinal oscillations with a period of approximately 300 s. The lower part of the slit position is lying (in projection) in such a manner obliquely that it detects the sloshing back and forth plasma on these tubes. Since this behavior is not evident in the Hα time-distance diagram, its origin is not in the lower solar atmosphere and it is most likely generated during the flare energy released in the overlying magnetic flux structure (Fig. 8). After repeating one cycle of the back and forth motion, finally part of the plasma starts downflowing through the magnetic channels with almost the same subsonic speed towards the penumbra of the sunspot lying northward. It should be noted that some plasma has already started flowing (the first linearly fitted envelope), while the rest will flow with almost the same velocity after the oscillations (see the nearly same slope in the in-bound envelope in the distance-time diagram). However, the longitudinal oscillations may not be the real oscillation signals, since only limited periods are detected. The alternative possibility is that the longitudinal oscillations result from repetitive flows triggered by continuous magnetic reconnections.

We note an interesting point that in Hα, the plasma instantly started flowing with supersonic speed through the superpenumbral magnetic channel ($t = 200$ s; first column in Fig. 6). However, in the transition region/inner coronal bands, part of the plasma flows in the same magnetic channel with a time lag of almost 200 s ($t = 400$ s; second-fourth columns in Figure 6). This indicates a very complex situation on the magnetic channel associated with the inverse Evershed effects, which may consist of the complex pattern of the flow of multi-temperature plasma with a range of downflow speeds. Moreover, they will also depend upon local magnetic field and plasma configuration and strength of the flare energy released (if any). Therefore, the multi-temperature and multi-height view of the inverse Evershed effect must be investigated in order to explore its underlying physical processes.

In spite of all its complexities, the plasma flows towards the inverse Evershed channel over the penumbra of the sunspot. The discontinuity in the typical magnetic field and plasma properties at the adjoining of these two different sets of field lines (superpenumbra and spot's penumbra) further leads to the discontinuity in characteristic magnetoacoustic and Alfvén speeds at the junction. This may further trap and stop the multi-temperature and mixed plasma flows that we observe in the present observational baseline. Future study will be devoted to identifying the inverse Evershed flow channels associated with the variety of flaring events, and constraining their multi-temperature and multi-height descriptions.

Acknowledgements One of the authors, DPC, gratefully acknowledges a travel grant from the Chinese Academy of Sciences to NAOC, where he completed a part of this work. The work is funded by the Chinese Academy of Science President's International Fellowship Initiative. *Hinode* is a Japanese mission developed and launched by ISAS/JAXA, collaborating with NAOJ as a domestic partner, and NASA and STFC (UK) as international partners. Scientific operation of the *Hinode* mission is conducted by the *Hinode* science team organized at ISAS/JAXA.

References

Antonucci, E., Dodero, M. A., & Martin, R. 1990, ApJS, 73, 137

Balasubramaniam, K. S., Pevtsov, A., & Rogers, J. 2004, ApJ, 608, 1148

Beck, C., Choudhary, D. P., & Rezaei, R. 2014, ApJ, 788, 183

Bellot Rubio, L. R., Tsuneta, S., Ichimoto, K., et al. 2007, ApJ, 668, L91

Benz, A. O. 2008, Living Reviews in Solar Physics, 5, 1

Choudhary, D. P., Ambastha, A., & Ai, G. 1998, Sol. Phys., 179, 133

Doyle, J. G., Ishak, B., Ugarte-Urra, I., Bryans, P., & Summers, H. P. 2005, A&A, 439, 1183

Falconer, D. A., Moore, R. L., Gary, G. A., & Adams, M. 2009, ApJ, 700, L166

Fletcher, L. 2010, Mem. Soc. Astron. Italiana, 81, 616

Forbes, T. G. 2003, Advances in Space Research, 32, 1043

Gary, G. A., & Moore, R. L. 2004, ApJ, 611, 545

Georgakilas, A. A., Christopoulou, E. B., Skodras, A., & Koutchmy, S. 2003, A&A, 403, 1123

Hagyard, M. J., & Rabin, D. M. 1986, Advances in Space Research, 6, 7

Hahn, M., Gaard, S., Jibben, P., Canfield, R. C., & Nandy, D. 2005, ApJ, 629, 1135

Ichimoto, K., Shine, R. A., Lites, B., et al. 2007, PASJ, 59, S593

Kitiashvili, I. N., Kosovichev, A. G., Wray, A. A., & Mansour, N. N. 2009, ApJ, 700, L178

Kosugi, T., Matsuzaki, K., Sakao, T., et al. 2007, Sol. Phys., 243, 3

Lemen, J. R., Title, A. M., Akin, D. J., et al. 2012, Sol. Phys., 275, 17

Liu, Z., Xu, J., Gu, B.-Z., et al. 2014, RAA (Research in Astronomy and Astrophysics), 14, 705

Louis, R. E., Beck, C., Mathew, S. K., & Venkatakrishnan, P. 2014, A&A, 570, A92

Martínez Pillet, V. 2000, A&A, 361, 734

Pesnell, W. D., Thompson, B. J., & Chamberlin, P. C. 2012, Sol. Phys., 275, 3

Rueedi, I., Solanki, S. K., & Rabin, D. 1992, A&A, 261, L21

Schad, T. A., Penn, M. J., & Lin, H. 2013, ApJ, 768, 111

Schad, T. A., Penn, M. J., Lin, H., & Tritschler, A. 2015, Sol. Phys., 290, 1607

Schlichenmaier, R., & Schmidt, W. 1999, A&A, 349, L37

Schou, J., Scherrer, P. H., Bush, R. I., et al. 2012, Sol. Phys., 275, 229

Shibata, K., & Magara, T. 2011, Living Reviews in Solar Physics, 8, 6

Solanki, S. K., Rueedi, I. K., & Livingston, W. 1992, A&A, 263, 312

Teriaca, L., Curdt, W., & Solanki, S. K. 2008, A&A, 491, L5

Thomas, J. H. 2002, Nature, 420, 134

Tsuneta, S., Ichimoto, K., Katsukawa, Y., et al. 2008, Sol. Phys., 249, 167

Vissers, G., & Rouppe van der Voort, L. 2012, ApJ, 750, 22

Wang, H., Jing, J., Tan, C., Wiegelmann, T., & Kubo, M. 2008, ApJ, 687, 658

Weigelt, G. P. 1977, Optics Communications, 21, 55

Westendorp Plaza, C., del Toro Iniesta, J. C., Ruiz Cobo, B., et al. 1997, Nature, 389, 47